Chinese Journal of Chemical Engineering 90 (2026) 196–202

Contents lists available at ScienceDirect

Chinese Journal of Chemical Engineering

journal homepage: www.elsevier.com/locate/CJChE

Full Length Article

High activity in alkylation of benzene and 1-dodecene over MOR zeolite nanorods

Junning Lu [1], Xuming Cai [1], Huali Zhang [1], Yi Huang [2], Baoyu Liu [1, 3, *]

[1] School of Chemical Engineering and Light Industry, Guangdong University of Technology, Guangzhou 510006, China
[2] School of Engineering, Institute for Materials & Processes, The University of Edinburgh, Edinburgh EH9 3FB, United Kingdom
[3] Guangdong Provincial Laboratory of Chemistry and Fine Chemical Engineering Jieyang Center, Jieyang 515200, China

ARTICLE INFO

Article history:
Received 12 July 2025
Received in revised form
16 September 2025
Accepted 17 September 2025
Available online 17 October 2025

Keywords:
Alkylation
MOR zeolite
Catalysis
Template

ABSTRACT

The development of green alkylation technology in the production of linear alkylbenzene based on zeolites is highly desired. Herein, a novel nanorod-like mordenite (MOR) zeolite is fabricated by employing a self-designed template, and the morphology of MOR zeolites can be tailored by tuning the alkalinity of the synthesis gel. It's pointed out that the specially designed template is composed of an ethylenediamine functional group and hydrophobic alkyl chains, and the aromatic-aromatic stacking interactions in hydrophobic alkyl chains may facilitate the self-assembly of micellar structures, while the ethylenediamine functional group is matched with building blocks of MOR zeolite, resulting in the formation of nanorod-like MOR zeolite. Moreover, it's demonstrated that the compact stacking nanorod-like particles can be transformed into loose nanorod-like morphology under high alkalinity conditions, in which the Si-O bands are depolymerized, leading to the exfoliation of the stacking nanorod-like particles. The resultant nanorod-like MOR zeolite (MOR-30) displays enhanced accessibility for Brønsted acid sites compared with conventional MOR, achieving over twice the catalytic activity of conventional MOR in the alkylation of benzene with 1-dodecene.

1. Introduction

Mordenite (MOR) zeolite is a significant catalyst employed in many petrochemical and petroleum refining processes, including reforming, alkylation, isomerization, and catalytic cracking [1,2]. The MOR zeolite contains a 12-membered ring (12-MR) main channels (0.65 nm × 0.70 nm) and a parallel 8-membered ring (8-MR) channel (0.26 nm × 0.57 nm) along the *c* axis. These channels are interconnected by an 8-MR channel (0.34 nm × 0.48 nm) oriented along the *b*-axis [3–5]. Because MOR zeolites have a limited number of 8-MR channels, those bulk-molecule reactions only occur in the 12-MR channels. Based on previous reports [6], the MOR zeolite shows exceptional catalytic performance in benzene alkylation with long-chain α-olefins, achieving high activity and remarkable selectivity of 2-alkylbenzene (2-LAB). The 2-LAB is the most biodegradable and environmentally superior among linear alkylbenzene isomers [7]. Therefore, it's crucial to develop an environmentally friendly solid acid catalyst with greater selectivity of 2-LAB in the alkylation reaction of benzene with 1-dodecene. Typically, MOR zeolite exhibits 2-LAB selectivity (~75%) owing to its distinct straight 12-MR channels [8]. However, the alkylation of benzene and long-chain α-olefins is hindered by diffusion restrictions caused by the narrow pore structure of traditional MOR zeolites. Thus, MOR zeolite's rapid deactivation presents a considerable challenge for its practical application in alkylbenzene manufacturing [9,10]. Han *et al.* [11] report that zeolitic channel obstruction by linear alkylbenzene and poly-aromatic compounds is the dominant deactivation mechanism in benzene/1-dodecene alkylation. While the nano-assembled MOR zeolites are fabricated to address the deactivation issues of zeolite catalysts, because their small grains offer a large specific surface area, low diffusion resistance, and short channels, which effectively enhance anti-coking performance.

Nano-assembled zeolites have a smaller crystal size in at least one dimension, which shortens diffusion pathways within the channels. The synthesis of nano-assembled MOR zeolite typically requires the utilization of organic templates. By using organic templates, the strong structure-directing effects govern the initial nucleation and subsequent crystal growth of zeolites [12–16]. In recent years, researchers have focused on developing both

* Corresponding author. School of Chemical Engineering and Light Industry, Guangdong University of Technology, Guangzhou 510006, China.
E-mail address: baoyu.liu@gdut.edu.cn (B. Liu).

https://doi.org/10.1016/j.cjche.2025.09.013

disordered and ordered nanocrystalline MOR zeolites to minimize diffusion path lengths, and various organic templates have been developed to synthesize the hierarchical zeolites [17–19], it's important to control the morphology of zeolites by tuning the molecular structure of organic templates. In view of this, we report a unique method for creating nanorod-like MOR zeolites with controlled morphology using an organic template that has been carefully designed. The alkalinity of the synthesis gel can be modulated to tailor the morphology of these zeolites. More importantly, the nanorod-like MOR zeolites exhibit significantly enhanced catalytic activity and stability compared with conventional MOR zeolites, and this work examines how zeolitic morphology affects catalytic performance.

2. Experimental

2.1. Synthesis of organic template

The specially designed organic template (H_2N-$(CH_2)_2$-NH-$(CH_2)_{12}$-*O*-C_6H_4-C_6H_4-*O*-$(CH_2)_{12}$-NH-$(CH_2)_2$-NH_2) is prepared by assembling the long-chain alkyl group and functional ammonium groups. Firstly, 10.75 mmol of 4,4′-biphenol and 54 mmol of 1,12-dibromododecane, and 22.81 mmol of potassium hydroxide are dissolved in 80 mL of ethanol, and the resulting mixture is stirred and refluxed at 80 °C for 20 h. The product is collected by precipitation, cooled to room temperature, and subsequently washed multiple times with ethanol. The intermediate product (Br-$(CH_2)_{12}$-*O*-C_6H_4-C_6H_4-*O*-$(CH_2)_{12}$-Br) is obtained, named as $C_{Ph\text{-}12\text{-}6}$.

Secondly, 20 mmol of $C_{Ph\text{-}12\text{-}6}$ and 250 mmol of ethylenediamine, and 21.5 mmol of potassium hydroxide are dissolved in a mixture of toluene-acetonitrile (1:1 by volume), followed by refluxing at 70 °C for 10 h, the resulting product of (H_2N—$(CH_2)_2$—NH—$(CH_2)_{12}$—O—C_6H_4—C_6H_4—O—$(CH_2)_{12}$—NH—$(CH_2)_2$—NH_2) is washed with diethyl ether, and it's named $C_{Ph\text{-}2\text{-}12\text{-}6}$, and the synthesis process can be founded in Scheme S1 in Supplementary Material, the molecular structure of obtained $C_{Ph\text{-}2\text{-}12\text{-}6}$ is characterized a with ^{1}H NMR in $CDCl_3$, as shown in Fig. S1.

2.2. Synthesis of catalysts

For the synthesis of MOR zeolites. First of all, 1.5 mmol of sodium hydroxide and 0.05 mmol of aluminium sulfate octadecahydrate, and 0.075 mmol of $C_{Ph\text{-}2\text{-}12\text{-}6}$ are dissolved in deionized water (75.83 mmol), after stirring for 0.5 h, TEOS (1.5 mmol) is added to the mixture. The resulting gel composition has a molar ratio of *x* NaOH:1 $Al_2(SO_4)_3 \cdot 18H_2O$:30 TEOS:1517$H_2O$: 1.5 $C_{Ph\text{-}2\text{-}12\text{-}6}$ ($x = 28$, 29, and 30 by tuning the amount of sodium hydroxide, respectively), which is aged at 50 °C for 24 h. Finally, the synthesis is performed on the final gel at 150 °C for 144 h. The obtained solids are washed and dried (100 °C, 12 h), and these obtained samples are denoted as MOR-*x* (MOR-28, MOR-29, and MOR-30 based on the above value of *x*), the synthesis process is shown in Scheme S2.

2.3. Catalytic tests

The Supporting Information contains the catalytic evaluation of nanorod-like MOR zeolites in the alkylation of benzene with 1-dodecene.

3. Results and Discussion

3.1. Catalyst characterization

The XRD spectrum of various MOR zeolites are shown in Fig. 1, all samples display the characteristic peaks at $2\theta = 6.51°$, 9.77°, 13.45°, 22.20°, 25.63°, 26.25° and 27.67° (the reference XRD pattern for MOR zeolite (PDF#80-0645) is displayed at the base of Fig. 1) [20], which is attributed to (1 1 0), (2 0 0), (1 1 1), (1 5 0), (2 0 2), (3 5 0), and (5 1 1) reflections of typical MOR zeolites, respectively. However, the resultant MOR-*x* samples show inferior intensity of the diffraction peaks compared with conventional MOR (C-MOR) due to the limited structure-directing capability of the organic template ($C_{Ph\text{-}2\text{-}12\text{-}6}$). In addition, the low-angle XRD patterns of all MOR-*x* samples display distinct peaks that could be assigned to additional mesopores. In contrast, C-MOR lacks low-angle reflections owing to its three-dimensional (3D) structure [18].

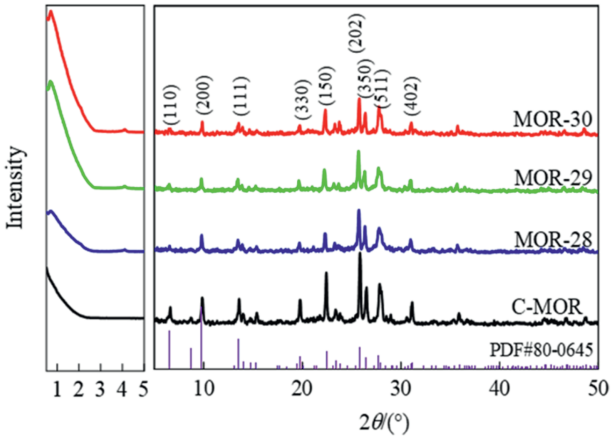

Fig. 1. Low-angle and High-angle XRD patterns of different MOR zeolites.

The N_2 adsorption-desorption isotherms reveal distinct curves for MOR zeolites. As shown in Fig. 2, C-MOR zeolite exhibits a type I adsorption isotherm, which is attributed to its primarily microporous structure [21]. For the MOR-*x* zeolites, all samples show a type IV isotherm with an additional hysteresis loop. Moreover, the synthesized MOR-*x* zeolites exhibit substantially improved textural characteristics, giving a higher external surface area and mesoporosity compared with C-MOR (Table 1). Notably, MOR-30 exhibits the highest mesopore volume and external surface area, indicating that the gel alkalinity during synthesis can significantly influence the textural parameters of MOR zeolites.

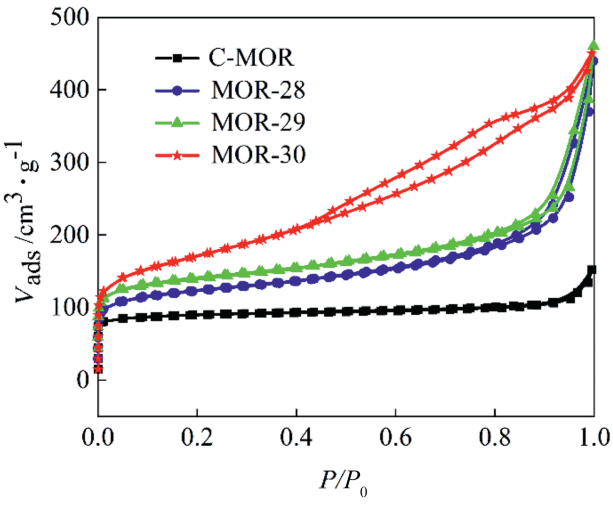

Fig. 2. N_2 adsorption-desorption isotherms of various MOR zeolites.

Table 1
Textural properties of various MOR zeolites.

Catalysts	S_{BET}[①]/$m^2 \cdot g^{-1}$	S_{ext}/$m^2 \cdot g^{-1}$	S_{micro}/$m^2 \cdot g^{-1}$	V_{tol}[②]/$cm^3 \cdot g^{-1}$	V_{micro}[③]/$cm^3 \cdot g^{-1}$	V_{meso}[④]/$cm^3 \cdot g^{-1}$
C-MOR	351	21	330	0.236	0.132	0.104
MOR-28	474	179	295	0.648	0.126	0.522
MOR-29	506	158	347	0.672	0.111	0.561
MOR-30	605	213	392	0.696	0.094	0.602

① Total surface of area was obtained by Brunauer–Emmett–Teller (BET) method.
② Determined from adsorbed volume at $P/P_0 = 0.99$.
③ Determined from t-plot method.
④ $V_{meso} = V_{tol} - V_{micro}$.

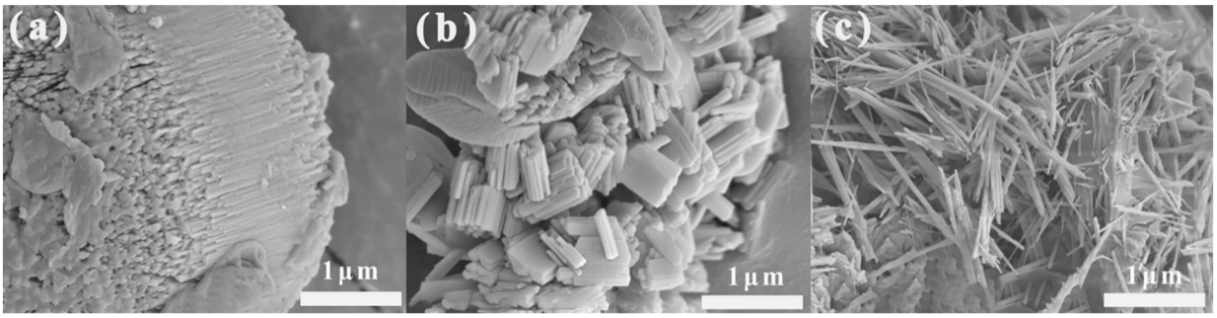

Fig. 3. SEM images of MOR-28 (a), MOR-29 (b), MOR-30 (c), respectively.

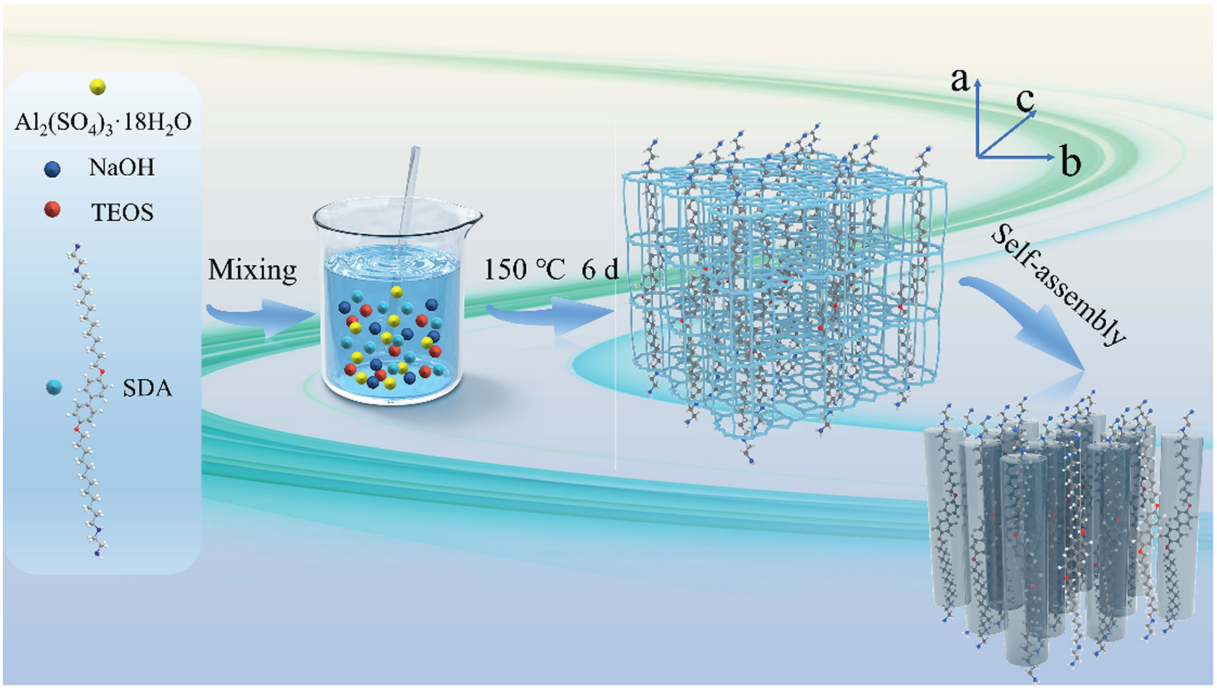

Fig. 4. Schematic diagram of the proposed structure mode for nanorod-like MOR zeolite.

Fig. 3 and Fig. S2 display SEM (scanning electron microscopy) images of C-MOR and MOR-*x* zeolites. It's noted from Fig. 3 that all the samples exhibit a nanorod-like morphology, which is attributed to the specially designed template. It's proposed that the benzene rings as the rigid segments in the template can stabilize the micelle structure through the aromatic–aromatic stacking interactions based on the previous study [22], which can inhibit the zeolitic growth by forming a stable hydrophobic layer. While the ethylenediamine functional group guides the formation of MOR zeolite framework as the role of template, resulting in the generation of nanorod-like MOR zeolite, and the proposed structure mode for nanorod-like MOR zeolite is listed in Fig. 4. Moreover, the MOR-*x* zeolite is transformed from compact stacking nanorod-like particles (Fig. 3(a)) into loose nanorod-like morphology (Fig. 3(b)), and the single nanorod MOR zeolite is produced at last (Fig. 3(c)). Based on our previous report [23], the high alkalinity is benefit for the depolymerization of $\equiv Si-O-Si\equiv$ species through the $\equiv Si-O-Si\equiv + OH^- \rightleftharpoons \equiv Si-$

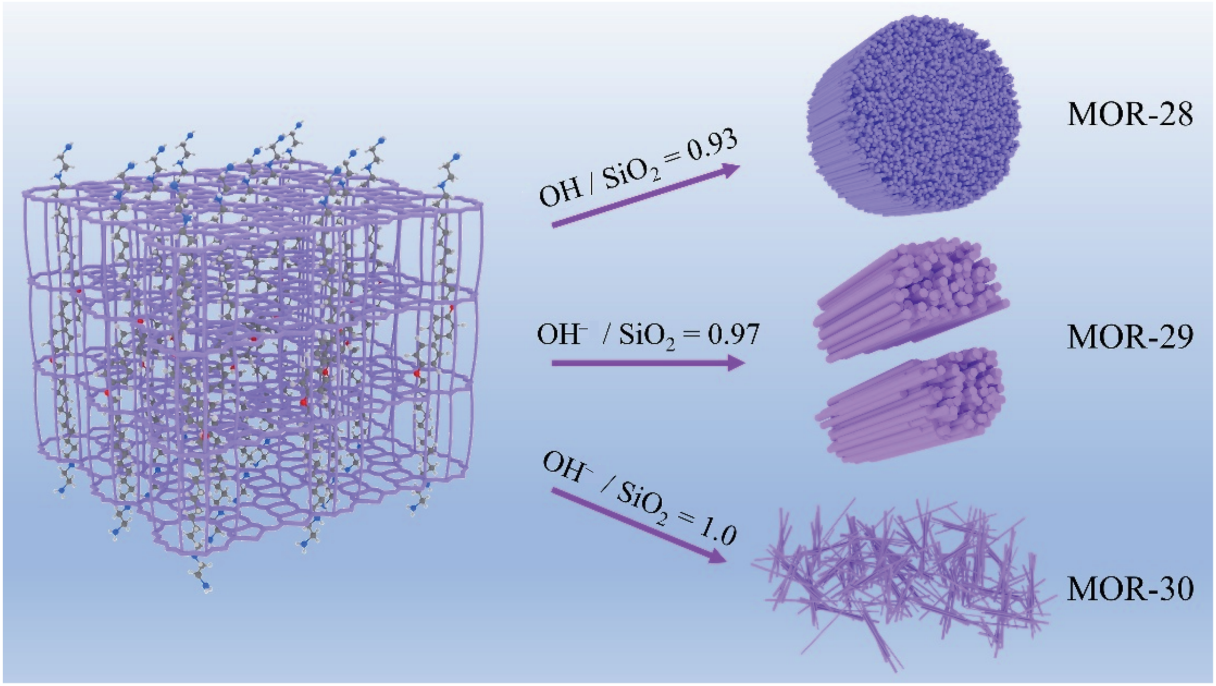

Fig. 5. Schematic diagram of the proposed regulation process for morphology of MOR zeolites.

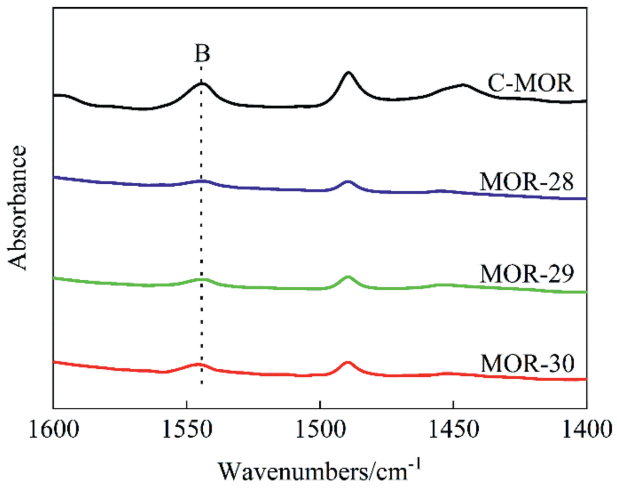

Fig. 6. FT-IR spectra of pyridine adsorption over different MOR-*x* zeolites.

$OH + \equiv Si - O^-$, resulting in the exfoliation of stacking nanorod-like particles, and the proposed regulation process for morphology of MOR zeolites is present in Fig. 5. On the contrary, the C-MOR displays bulky crystal morphology (Fig. S2).

Fig. 6 and Table S1 present the FT-IR spectra for pyridine adsorption over various MOR zeolites as well as the detailed acidity of the resultant MOR zeolites. It's observed from Fig. 6 and Table S1 that total Brønsted acid sites increased with increasing alkalinity, indicating that the alkalinity is also an important factor influencing Brønsted acidity. To investigate which type of acid site of MOR zeolite dominates the reaction activity in the alkylation reaction, the poisoning experiment is carried out with typical MOR-30 adsorbed by pyridine, 2,6-ditert-butylpyridine and MOR-30 after ion exchange with sodium chloride (Fig. S3), these results demonstrate that external Brønsted acid sites serve as the primary active sites.

In our previous work [23], we point out that Na^+ plays an important role in balancing the negative aluminosilicate species in the aluminum-rich synthesis gel, and the $[AlO_4]^-$ species can interact with Na^+ ions through electrostatic interaction, which introduces more Al species into the framework of MOR zeolites as the amount of NaOH in the synthesis gel increases. Thus, the Si/Al ratio of MOR-*x* decreases with increasing alkalinity, while the concentration of Brønsted acid sites increases in the order of MOR-28 < MOR-29 < MOR-30 (Table S1). Moreover, the C-MOR exhibits the greatest concentration of Brønsted acid sites due to its low Si/Al ratio and integrated microporous structure [18,24]. In addition, the external Brønsted acid sites are marked by the characteristic absorption peak of 2,6-di-*tert*-butylpyridine at 1616 cm^{-1} [25], as shown in Fig. S4. The MOR-*x* exhibits the highest density of external Brønsted acid sites compared with C-MOR, due to its highly open hierarchical structure. Furthermore, the concentrations of external Brønsted acid sites for the MOR-*x* increase in the order of MOR-28 < MOR-29 < MOR-30 (Table S1), indicating that the acid distributions of MOR-*x* samples can be tailored by tuning the alkalinity, which is beneficial for alkylation between benzene and 1-dodecene.

3.2. The catalytic performances of obtained MOR zeolites

The catalytic performance of the MOR zeolites in the alkylation of benzene and 1-dodecene is investigated, as shown in Fig. 7. The C-MOR zeolite exhibits the lowest activity although it has the highest density of Brønsted acid sites that are the main active sites (Fig. 7(a)) [26], indicating that the narrow pore structure of traditional MOR zeolites imposes significant diffusion constraints, thereby inhibiting the alkylation process between benzene and 1-dodecene. Interestingly, the activity of MOR-*x* samples increases in the order of MOR-28 < MOR-29 < MOR-30, which is in agreement with the density of external Brønsted acid sites of MOR-*x* zeolites listed in Table S1. These data demonstrate that the fabrication of nanorod-like particles significantly improves the diffusion

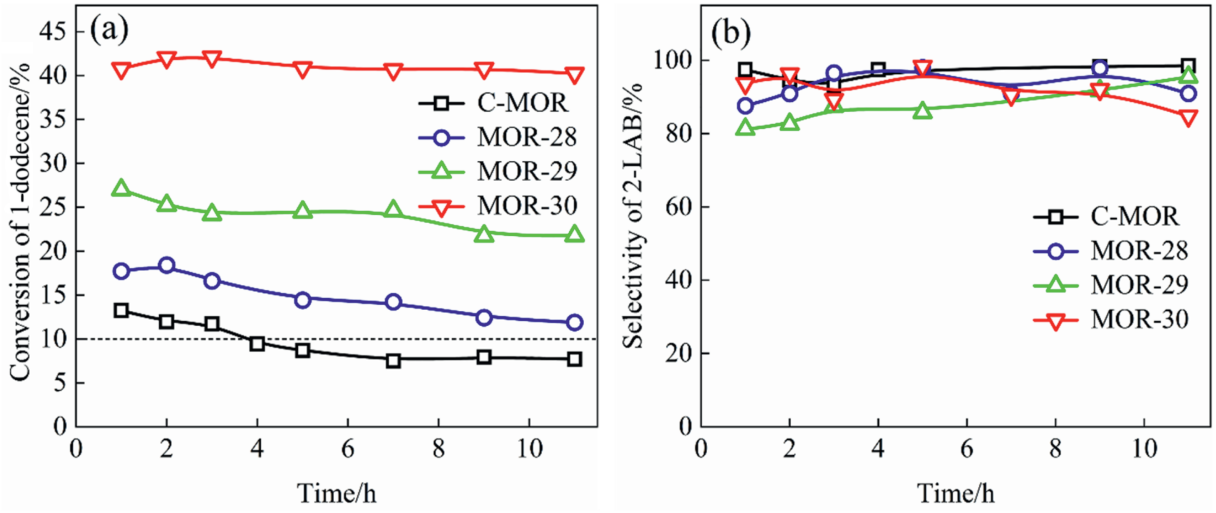

Fig. 7. Conversion of 1-Dodecene (a) and selectivity of 2-LAB (b) of MOR zeolites; Reaction conditions: molar ratio of benzene/1-dodecene = 10; T = 80 °C; WHSV = 20 h^{-1}.

properties of the MOR-*x* zeolites. In addition, all MOR zeolites exhibit comparable selectivity of 2-LAB, which is attributed to their straight 12-MR channels that are matched with 2-LAB molecules [27–29]. In contrast, the MOR-29 presents an inferior selectivity of 2-LAB due to its inhomogeneous morphology that might influence the diffusion of LAB isomers (Fig. 7(b)). Furthermore, the nanorod-like MOR zeolite also exhibits higher catalytic activity compared to other typical zeolites with a 12-MR structure, such as MWW, Beta zeolites, as shown in Fig. S5. Moreover, Fig. S6 and Table S2 provide the thermogravimetric (TG) data of spent C-MOR and MOR-*x*, it's found from Table S2 that the coke deposition rate increases in the order of MOR-30 < MOR-29 < MOR-28 < C-MOR, suggesting that the obtained MOR-30 possesses superior diffusion performance that can inhibit the formation of coke species. Furthermore, the C-MOR has low concentration of external Brønsted acid sites (Table S1), which means that most of Brønsted acid sites are located in the interior of C-MOR, resulting in the accumulation of coke precursor species owing to diffusion limitation, these coke species can form the hard coke or soft coke at last. While the coke deposition rate gradually decrease with increasing the density of external Brønsted acid sites, indicating that the high accessibility of Brønsted acid sites can inhibit the formation of coke species.

Furthermore, the hydrocarbon compositions in typical C-MOR and MOR-30 after reaction are analyzed by GC-MS (Fig. 9). It can be seen that the compounds are highly complicated, indicating that the complex reaction pathways are involved in this alkylation process, in which the 1-dodecene is activated as the carbenium ion on the Brønsted acid site, then it undergo rapid secondary rearrangements to react with benzene, leading to the formation of

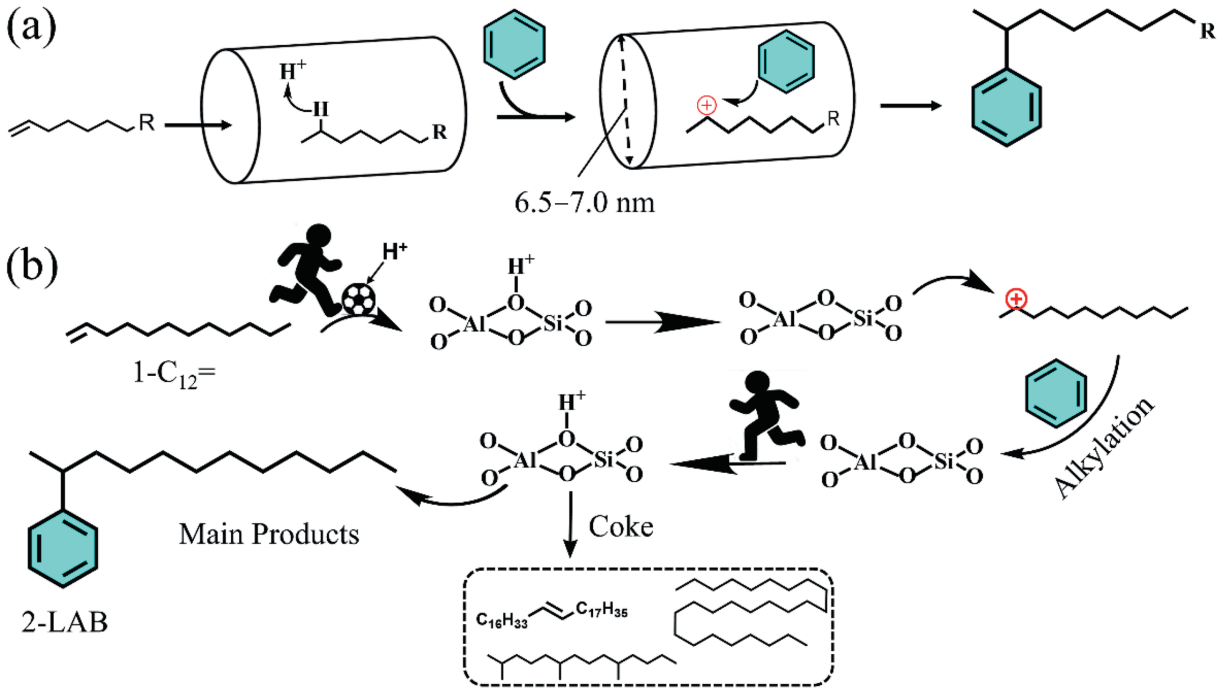

Fig. 8. The alkylation between benzene and 1-dodecene (a) and proposed reaction network (b).

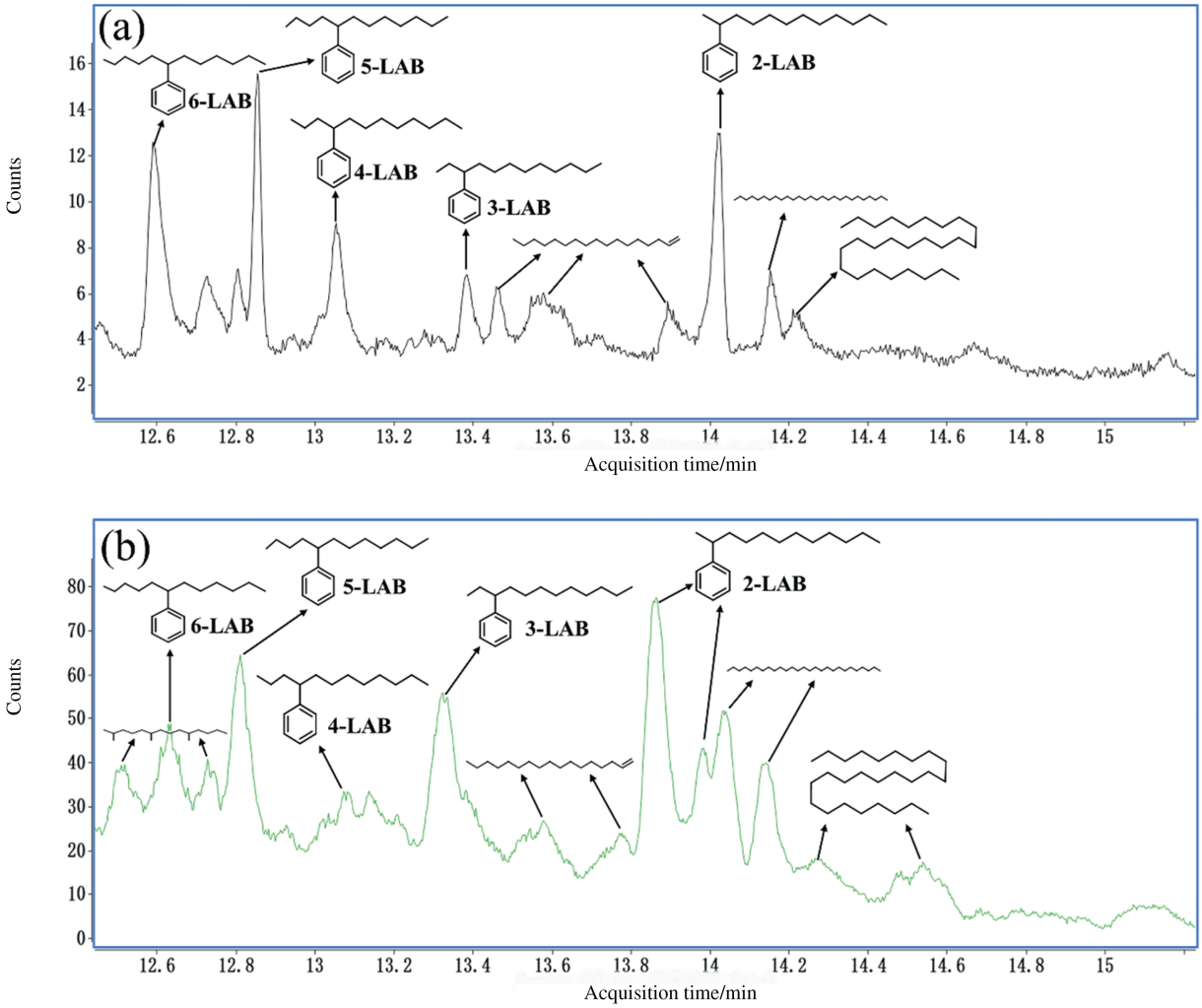

Fig. 9. GC-MS spectrogram of (a) spent C-MOR and (b) spent MOR-30.

alkylbenzenes with various isomers [29,30]. while the l-LAB is absent since primary carbenium ions exhibit a much lower stability than secondary carbenium ions [31]. In addition, the cracking and oligomerization of olefins occur as side reactions, which can cause the blockage of zeolitic channels, resulting in the deactivation of catalysts. Based on the above analyses, the proposed reaction network for the alkylation between benzene and 1-dodecene is illustrated in Fig. 8.

3.3. The regeneration performance of MOR zeolites

To further investigate the structural stability of the MOR zeolite, the spent MOR zeolites are regenerated, and the crystal structure of these regenerated MOR zeolites is characterized by XRD spectra, as shown in Fig. S7. It is observed that the XRD patterns between fresh and regenerated MOR zeolites have no significant changes, demonstrating that the framework structure of MOR zeolites is well maintained in the regeneration process. Furthermore, Fig. S8 displays the catalytic activity of regenerated C-MOR and MOR-30 samples in alkylation, it's found that the selectivity of 2-LAB is maintained due to its distinctive 12-MR pore structure [30,32]. Based on the acid data of regenerated and fresh MOR zeolites, as determined from Fig. S9 and Table S1, the density of Brønsted acid sites in Re-MOR-30 and Re-C-MOR is reduced compared to fresh MOR-30 and C-MOR, respectively, leading to inferior activity of regenerated MOR zeolites (Fig. S8). Specially, the regeneration process maintains ~47% of Brønsted acid sites in Re-C-MOR, but only ~9% acidity is lost for Re-MOR-30 in regeneration process, which means that the resultant MOR-30 has good regeneration performance compared with C-MOR owing to its unique nanorod structure, and the regeneration process need be optimized in the further work in order to completely recover the acidity of MOR zeolites.

4. Conclusions

In conclusion, the nanorod-like MOR zeolite is successfully synthesized by employing a specially designed template ($C_{Ph\text{-}2\text{-}12\text{-}6}$), and the morphology of nanorod-like MOR zeolite is tailored by tuning the alkalinity of the synthesis gel, resulting in the formation of single-nanorod MOR zeolite through the depolymerization of $\equiv Si-O-Si\equiv$ species, which not only improve the accessibility of Brønsted acid sites, but also enhance the diffusion of coke species in the framework of MOR zeolites, leading to the superior catalytic performance of resultant MOR-30 in benzene/1-dodecene alkylation. These studies can directly contribute to an insight into the

structure-property relationship between zeolitic structure and catalytic properties of the alkylation reaction. Besides, these findings also provide important guidance for the catalyst design and regulation of zeolite morphology.

CRediT Authorship Contribution Statement

Junning Lu: Writing – original draft. Xuming Cai: Methodology. Huali Zhang: Visualization. Yi Huang: Resources. Baoyu Liu: Writing – review & editing, Supervision.

Declaration of Competing Interest

We declare that we have no financial and personal relationships with other people or organizations that can inappropriately influence our work, there is no professional or other personal interest of any nature or kind in any product, service and/or company that could be construed as influencing the position presented in, or the review of, the manuscript entitled.

Acknowledgements

This work is supported by National Natural Science Foundation of China (22278090 and 21978055).

Supplementary Material

Supplementary data to this article can be found online at https://doi.org/10.1016/j.cjche.2025.09.013.

References

[1] B. Wang, C.W. Lee, T.X. Cai, S.E. Park, Benzene alkylation with 1-dodecene over H-mordenite zeolite, *Catal. Lett.* 76 (1) (2001) 99–103.
[2] J. Yao, Y. Wang, S.S. Bello, G.W. Xu, L. Shi, Regulation of Brønsted acid sites in H-MOR for selective methyl methoxyacetate synthesis, *Appl. Organomet. Chem.* 34 (11) (2020) e5925.
[3] Z.Z. Cheng, S.Y. Huang, Y. Li, J. Lv, K. Cai, X.B. Ma, Deactivation kinetics for the carbonylation of dimethyl ether to methyl acetate on H-MOR, *Ind. Eng. Chem. Res.* 56 (46) (2017) 13618–13627.
[4] H.D. Wang, F. Jiao, J.Y. Feng, Y.C. Zhang, Z.C. Xu, X.L. Pan, X.H. Bao, Maximizing the accessibility of acid sites within zeolite catalysts for syngas conversion, *Angew. Chem. Int. Ed.* 64 (18) (2025) e202424946.
[5] N.B. Abdul Rahman, I. Alalq, M.J. Wulfers, D.K. Nielsen, D.E. Resasco, S.P. Crossley, Lanthanum incorporation in H-MOR zeolite to improve shape selectivity and stability against coke formation during the alkylation of toluene with isopropanol, *Appl. Catal. Gen.* 695 (2025) 120150.
[6] H.T. Yen, J.J. Wang, S.H. Siao, S.H. Cha, S.B. Hong, S.S. Al-Khattaf, I. Wang, T.C. Tsai, Design of an MWW zeolite catalyst for linear alkylbenzene synthesis with improved catalytic stability, *Catal. Sci. Technol.* 6 (8) (2016) 2715–2724.
[7] A. Aitani, J.B. Wang, I. Wang, S. Al-Khattaf, T.C. Tsai, Environmental benign catalysis for linear alkylbenzene synthesis: a review, *Catal. Surv. Asia* 18 (1) (2014) 1–12.
[8] W. Aslam, M.A.B. Siddiqui, B. Rabindran Jermy, A. Aitani, J. Čejka, S. Al-Khattaf, Selective synthesis of linear alkylbenzene by alkylation of benzene with 1-dodecene over desilicated zeolites, *Catal. Today* 227 (2014) 187–197.
[9] O.V. Shvets, K.M. Konysheva, M.M. Kurmach, Morphology and catalytic properties of hierarchical zeolites with MOR, BEA, MFI, and MTW topology, *Theor. Exp. Chem.* 54 (2) (2018) 138–145.
[10] J. Liang, Y.Y. Wang, X.C. Li, M. Xu, S.C. Shen, C. Liu, W.H. Fu, W.C. Tao, Z.Q. Yuan, Z.D. Wang, W.M. Yang, Synthesis of Al-BEC zeolite as an efficient catalyst for the alkylation of benzene with 1-dodecene, *Microporous Mesoporous Mater.* 328 (2021) 111448.
[11] C. Xu, M.H. Han, Z.H. Cui, Mechanism of deactivation and regeneration of β zeolite catalysts in alkyl benzene production, *Pet. Pro. Pet.* 3 (2002) 47–50.
[12] Y. Li, Z.H. Li, S.Y. Huang, K. Cai, Z. Qu, J.F. Zhang, Y. Wang, X.B. Ma, Morphology-dependent catalytic performance of mordenite in carbonylation of dimethyl ether: enhanced activity with high c/b ratio, *ACS Appl. Mater. Interfaces* 11 (27) (2019) 24000–24005.
[13] F. Chen, X.B. Feng, J.P. Zhao, Z.M. He, L.Y. Zhang, Y.H. Wang, P. Deng, X.H. Gao, X.Y. Zhao, J.P. Cao, Designing mordenite zeolites with tunable distribution of acid sites in channels and nano-morphology to boost the catalytic behavior performance of dimethyl ether carbonylation, *Chem. Eng. Sci.* 282 (2023) 119250.
[14] F. Chen, X.B. Feng, P. Deng, L.Y. Zhang, J.P. Zhao, Y.H. Wang, B.Y. Tao, X.Y. Zhao, J.P. Cao, H.C. Bai, Tailor-made the ultrathin nanosheet and acid site accessibility of mordenite zeolite for carbonylation of dimethyl ether, *Chem. Eng. J.* 498 (2024) 155451.
[15] W.R. Liu, Y.Q. Wang, L.Z. Bu, Y.Q. Zhi, Z.Q. Wang, M.Y. Yang, K.L. Chu, Y.T. Huang, N.D. Guo, L.P. Qu, J.C. Sang, Wheel-like mordenite nanoassemblies with shortened channel lengths for improved catalytic performance in dimethyl ether carbonylation, *ACS Appl. Nano Mater.* 6 (19) (2023) 18005–18015.
[16] M. Ma, X.M. Huang, E.S. Zhan, Y. Zhou, H.F. Xue, W.J. Shen, Synthesis of mordenite nanosheets with shortened channel lengths and enhanced catalytic activity, *J. Mater. Chem. A* 5 (19) (2017) 8887–8891.
[17] P. Rani, R. Srivastava, B. Satpati, One-step dual template mediated synthesis of nanocrystalline zeolites of different framework structures, *Cryst. Growth Des.* 16 (6) (2016) 3323–3333.
[18] M.N. Liu, Y.Z. Li, Z.X. Xie, Q.Q. Hao, Q.X. Luo, J.B. Zhang, H.Y. Chen, C.Y. Dai, X. X. Ma, Organosilane surfactant-directed synthesis of hierarchical mordenite with enhanced catalytic performance in the alkylation of benzene with 1-dodecene, *New J. Chem.* 44 (38) (2020) 16638–16644.
[19] O.V. Shvets, K.M. Konysheva, M.V. Shamzhy, M.V. Opanasenko, P.S. Yaremov, C.H. Xiao, X.D. Zou, J. Čejka, Mordenite nanorods and nanosheets prepared in presence of gemini type surfactants, *Catal. Today* 324 (2019) 115–122.
[20] J. Yao, X.B. Feng, J.Q. Fan, Y.L. He, R. Kosol, Y. Zeng, G.B. Liu, Q.X. Ma, G.H. Yang, N. Tsubaki, Effects of mordenite zeolite catalyst synthesis conditions on dimethyl ether carbonylation, *Microporous Mesoporous Mater.* 306 (2020) 110431.
[21] Y.H. Liu, N. Zhao, H. Xian, Q.P. Cheng, Y.S. Tan, N. Tsubaki, X.G. Li, Facilely synthesized H-mordenite nanosheet assembly for carbonylation of dimethyl ether, *ACS Appl. Mater. Interfaces* 7 (16) (2015) 8398–8403.
[22] D.D. Xu, Y.H. Ma, Z.F. Jing, L. Han, B. Singh, J. Feng, X.F. Shen, F.L. Cao, P. Oleynikov, H. Sun, O. Terasaki, S.N. Che, π-π interaction of aromatic groups in amphiphilic molecules directing for single-crystalline mesostructured zeolite nanosheets, *Nat. Commun.* 5 (2014) 4262.
[23] F. Xiong, C. Ji, S.Z. Gan, P. Liang, Y. Huang, J. Shang, B.Y. Liu, J.X. Dong, Tuning the mesoscopically structured ZSM-5 nanosheets for the alkylation between toluene and methanol, *AIChE J.* 69 (6) (2023) e18054.
[24] S. Tada, D.X. Li, M. Okazaki, H. Kinoshita, M. Nishijima, N. Yamauchi, Y. Kobayashi, K. Iyoki, Influence of Si/Al ratio of MOR type zeolites for bifunctional catalysts specific to the one-pass synthesis of lower olefins *via* CO_2 hydrogenation, *Catal. Today* 411-412 (2023) 113828.
[25] C.Y. Wang, K. Lu, F. Jin, G.Y. Wu, Y.C. Zhao, X. Yong, Modification of MWW layer structure to investigate the effect of acidity and Zn-type sites on ethane dehydroaromatization, *Catal. Today* 368 (2021) 250–259.
[26] B.Y. Liu, W.J. Lu, Y.K. Liu, Q.L. Feng, Y. Huang, J. Shang, Y.H. Zhu, J.X. Dong, Synthesis of dodecylbenzene *via* the alkylation of benzene and 1-dodecene over mesopore Beta zeolites, *AIChE J.* 69 (11) (2023) e18201.
[27] J.S. Lin, J.J. Wang, J. Wang, I. Wang, R.J. Balasamy, A. Aitani, S. Al-Khattaf, T.C. Tsai, Catalysis of alkaline-modified mordenite for benzene alkylation of diolefin-containing dodecene for linear alkylbenzene synthesis, *J. Catal.* 300 (2013) 81–90.
[28] R.M. Li, S.Y. Xing, S. Zhang, M.H. Han, Effect of surface silicon modification of H-beta zeolites for alkylation of benzene with 1-dodecene, *RSC Adv.* 10 (17) (2020) 10006–10016.
[29] J.J. Wang, Y.Y. Chuang, H.Y. Hsu, T.C. Tsai, Toward industrial catalysis of zeolite for linear alkylbenzene synthesis: a mini review, *Catal. Today* 298 (2017) 109–116.
[30] T. Pu, J.N. Lu, Z.R. Liu, X.X. Zeng, B.Y. Liu, Alkylation of benzene and 1-dodecene over cerium-silicate pillared MWW zeolite, *Chin. J. Chem. Eng.* 80 (2025) 110–118.
[31] S.Q. Zhang, S.Z. Gan, B.Y. Liu, J.X. Dong, Production of linear alkylbenzene over Ce containing Beta zeolites, *Chin. J. Chem. Eng.* 67 (2024) 220–227.
[32] B.Y. Liu, Z.T. Liao, Y. Wu, C.H. Ding, F.S. Butt, Y. Huang, J.X. Dong, Efficient production of linear alkylbenzene by liquid alkylation between benzene and 1-dodecene over MWW zeolites, *Mol. Catal.* 531 (2022) 112642.